Title

From the Cover: Thirdhand Cigarette Smoke Causes Stress-Induced Mitochondrial Hyperfusion and Alters the Transcriptional Profile of Stem Cells

Journal

Toxicological Sciences, 153(1)

ISSN

1096-6080

Authors

Bahl, Vasundhra
Johnson, Kimberly
Phandthong, Rattapol
et al.

Publication Date

2016-09-01

DOI

10.1093/toxsci/kfw102

Peer reviewed

OXFORD

SOT | Society of Toxicology
www.toxsci.oxfordjournals.org

TOXICOLOGICAL SCIENCES, 153(1), 2016, 55–69

doi: 10.1093/toxsci/kfw102
Advance Access Publication Date: June 2, 2016
Research article

Thirdhand Cigarette Smoke Causes Stress-Induced Mitochondrial Hyperfusion and Alters the Transcriptional Profile of Stem Cells

Vasundhra Bahl,*,† Kimberly Johnson,* Rattapol Phandthong,* Atena Zahedi,*,‡ Suzaynn F. Schick,§ and Prue Talbot*,[1]

*Department of Cell Biology and Neuroscience, University of California Riverside, Riverside, California 92521; †Environmental Toxicology Graduate Program University of California Riverside; ‡Bioengineering Interdepartmental Graduate Program, University of California Riverside; and §Division of Occupational and Environmental Medicine Department of Medicine, University of California, San Francisco, California 94243

[1]To whom correspondence should be addressed. Fax: 951-827-4286. E-mail: talbot@ucr.edu.

ABSTRACT

Thirdhand cigarette smoke (THS) was recently recognized as an environmental health hazard; however, little is known about it effects on cells. Mitochondria are sensitive monitors of cell health and report on environmentally induced stress. We tested the effects of low levels of THS extracted from terry cloth on mitochondrial morphology and function using stem cells with well-defined mitochondria. Concentrations of THS that did not kill cells caused stress-induced mitochondrial hyperfusion (SIMH), which was characterized by changes in mitochondrial morphology indicative of fusion, increased mitochondrial membrane potential (MMP), increased ATP levels, increased superoxide production, and increased oxidation of mitochondrial proteins. SIMH was accompanied by a decrease in *Fis1* expression, a gene responsible for mitochondrial fission, and a decrease in apoptosis-related genes, including *Aifm2*, *Bbc3*, and *Bid*. There was also down regulation of *Ucp2*, *Ucp4*, and *Ucp5*, genes that decrease MMP thereby reducing oxidative phosphorylation, while promoting glycolysis. These effects, which collectively accompany SIMH, are a prosurvival mechanism to rescue damaged mitochondria and protect cells from apoptosis. Prolonged exposure to THS caused a reduction in MMP and decreased cell proliferation, which likely leads to apoptosis.

Key words: thirdhand smoke; cigarette; smoke; tobacco; mitochondria; fusion; stress; oxidation; reactive oxygen species.

Mitochondria are vital organelles that function in ATP production, redox signaling, cell cycle regulation, differentiation, exchange of DNA between cells to restore function, and apoptosis (Collins *et al.*, 2012; Newmeyer and Ferguson-Miller, 2003; Tan *et al.*, 2008). They continually undergo fission for the disposal of defective mitochondria (Shen *et al.*, 2014) and fusion for exchange of mitochondrial DNA and rescue of damaged mitochondria (Chen *et al.*, 2010). There is a fine balance between fission and fusion in healthy cells. Any disruption of this dynamic balance can lead to compromised function (Otera *et al.*, 2013). The shape and size of mitochondria normally change through fission and fusion, and the internal structures of mitochondrial can be altered in response to physiological conditions (Detmer and Chan, 2007).

Mutations in mitochondrial DNA are responsible for numerous diseases such as optic atrophy (Zanna *et al.*, 2008), mitochondrial myopathy (Sweeney *et al.*, 1993), and diabetes mellitus (Gerbitz *et al.*, 1996). *OPA1* and *MFN2* mutations have been linked to neurodegenerative diseases such as optic atrophy and Charcot-Marie Tooth type 2A, respectively (Olichon *et al.*, 2006). Increased levels of the protein DRP1 (dynamin-like protein 1), which mediates outer mitochondrial membrane fission, are found in brains of Alzheimer's disease patients and increased mitochondrial fragmentation is also linked to Huntington's

disease (Chen and Chan, 2009). An imbalance in mitochondrial dynamics is implicated in type 2 diabetes, in which the β cells in the pancreas exhibit swollen mitochondria, impaired insulin production, reduced mitochondrial membrane potential (MMP), and reduced ATP production (Yoon *et al.*, 2011).

Mitochondria may be damaged by exposure to toxicants, and therefore serve as an excellent model for investigation of environmental chemicals (Meyer *et al.*, 2013). Effects produced by toxicants include inhibition of ATP synthesis due to uncoupling of oxidative phosphorylation (Wallace and Starkov, 2000), increased oxidative stress (Jia *et al.*, 2007), and mitochondria-initiated apoptosis (Stridh *et al.*, 1999). Sometimes in the presence of environmental stress, such as UV irradiation or actinomycin, mitochondria fuse to form a highly connected network through a process called stress-induced mitochondrial hyperfusion (SIMH) (Tondera *et al.*, 2009). This mechanism, which inactivates the fission machinery, protects cells against stress and prevents cell death (Shutt and McBride, 2013).

Cigarette smoke is an environmental toxicant that affects mitochondrial function. Some documented effects caused by cigarette smoke extracts include mitochondrial fragmentation in bronchial epithelial cells (Hara *et al.*, 2013) and alteration of mitochondrial structure and function in airway epithelium (Hoffmann *et al.*, 2013). Mitochondrial DNA mutations, including point mutations and insertions/deletions in the DNA sequence, have been reported in buccal cells of smokers that used at least 10 cigarettes/day for at least 6 months (Tan *et al.*, 2008). Low doses of cigarette smoke also cause a change in the morphology of mitochondria, giving rise to hyperfused networks which are thought to be an adaptive response to low levels of stress (Ballweg *et al.*, 2014).

Thirdhand cigarette smoke (THS), which consists of cigarette smoke residue that settles in indoor environments after smoking has occurred, has emerged as potential health hazard (Bahl *et al.*, 2014; Matt *et al.*, 2011). THS causes detrimental effects on cell health, such as DNA strand breaks in stem cells and adult cells (Bahl *et al.*, 2016a; Hang *et al.*, 2013), impairment of prenatal lung development in rats (Rehan *et al.*, 2011), and adverse effects on multiple organ systems of mice, including nonalcoholic fatty liver disease, excessive collagen production and increased inflammatory cytokines in the lungs, and delayed wound healing in the skin (Martins-Green *et al.*, 2014). Our studies have shown that volatile organic chemicals in THS are cytotoxic to stem cells and adult cells (Bahl *et al.*, 2016b). Acrolein, which was identified as the most potent of the volatile chemicals in THS, inhibited cell proliferation by altering expression of genes that regulate the cell cycle (Bahl *et al.*, 2016b).

Based on the above data, we hypothesized that THS damages mitochondria leading to cell morbidity and/or cell death. We tested this hypothesis using aqueous extracts of THS and mouse neural stem cells (mNSC). mNSC were chosen because they model the postnatal brain, which is a target of cigarette smoke (Dwyer *et al.*, 2009; Ernest *et al.*, 2001). In addition, mNSC have small spherical mitochondria that facilitate morphological and quantitative analysis of treatment-induced changes. THS was generated in a ventilated chamber by exposing terry cloth to cigarette smoke from Marlboro Red hardpack cigarettes as described previously (Bahl *et al.*, 2014). THS was extracted in cell culture medium, and cells were treated with varying concentrations of the extracts. We assessed effects on mitochondrial morphology, fusion, MMP, ATP production, reactive oxygen species (ROS) generation, oxidation of mitochondrial proteins, and the transcription of genes associated with mitochondrial function and stress. This is the first study that describes the effect of THS on mitochondrial dynamics, structure, and function and will provide valuable insight into how THS impacts mitochondrial processes and overall cell health.

MATERIALS AND METHODS

Generation of THS. THS was generated in an experimental chamber at the University of California San Francisco (UCSF) as described previously (Bahl *et al.*, 2014; Schick *et al.*, 2014). Terry cloth, prewashed as described previously (Bahl *et al.*, 2014) was exposed to cigarette smoke from approximately 133 Marlboro Red cigarettes over a span of 11 months. After exposure, terry cloth was wrapped in closed plastic bags and stored another 11 months. Fabric was then shipped to UCR where it was stored in amber bottles for another 15 months before extraction into culture medium. Two other batches of terry cloth were also exposed to cigarette smoke in the same experimental chamber. One batch was exposed to 11 cigarettes for 4 months and extraction was carried out within 1 week of removal from the chamber. The other batch was exposed to 75 cigarettes for 9 months and kept in the chamber for another 2 months to age, after which it was extracted. All the experiments except those labeled in Figure 3 as 11 cigarettes and 75 cigarettes, were done with THS extracts from terry cloth exposed to 133 cigarettes.

Preparation of THS extracts in culture medium. Aqueous extracts of THS were prepared in Dulbecco's Modified Eagle Medium (DMEM) as described previously (Bahl *et al.*, 2014). A known weight of unexposed or THS exposed terry cloth (0.125 g of fabric/ml of medium) was soaked in culture medium in 15 ml conical tubes. The tubes were subjected to constant agitation using a rotating shaker for 1 h at room temperature, after which the contents were transferred to a 3 ml plastic syringe (Sigma-Aldrich, St. Louis, Missouri) inside a fresh 15 ml conical tube which was centrifuged at 4000 × g for 5 min to recover the culture medium absorbed in the fabric. The recovered THS extracts were filtered through 0.22 μm sterile filters (Pall Corporation, Port Washington, New York), supplemented with fetal bovine serum (Sigma-Aldrich), horse serum (Invitrogen, Grand Island, New York), sodium pyruvate and penicillin-streptomycin, and aliquoted into 1.5 ml vials before storing at −80°C. For treating human embryonic stem cells (hESC), THS was extracted in mTeSR1 Medium (Stem Cell Technologies, Vancouver, BC, Canada) and frozen after addition of mTeSR supplement. All other steps during extraction were the same as described above.

Culturing mNSC. mNSC, which were generously provided by Dr Evan Snyder, were cultured in DMEM (Lonza, Walkersville, Maryland) containing 10% fetal bovine serum (Sigma-Aldrich), 5% horse serum (Invitrogen), 1% sodium pyruvate (Lonza), and 1% penicillin-streptomycin (GIBCO, Invitrogen) (Behar *et al.*, 2012a, b). The cells were cultured in Nunc T-25 tissue culture flasks (Fisher Scientific, Tustin, California) at 37°C, in 5% CO2 and 95% relative humidity. Medium was replaced on alternate days, and when confluency reached about 80%, cells were used in an experiment. To detach cells, plates were washed with Dulbecco's phosphate buffered saline (DPBS) then treated with 0.05% trypsin EDTA/DPBS (GIBCO, Invitrogen) for 1 min at 37°C.

Culturing hESC. H9 hESC obtained from WiCell (Madison, Wisconsin) were maintained on Matrigel (Fisher Scientific, Bedford, Massachusetts) coated 6-well plates (Falcon, Fisher

Scientific, Chino, California) containing complete mTeSR1 Medium (Stem Cell Technologies, Vancouver, BC, Canada) (Behar *et al.*, 2012a, b; Lin and Talbot, 2011). Cells were incubated in a 5% CO2 incubator at 37°C and 95% relative humidity. Each day cultures were observed for normal morphology, and medium was changed. Cells were used for experiments when they were 60%–80% confluent. To detach cells, wells were washed with DPBS (GIBCO, Invitrogen, Carlsbad, California), and colonies were enzymatically detached using Accutase (eBioscience, San Diego, California). Large cell clumps were mechanically broken using sterile glass beads, and cells were plated on Matrigel coated Ibidi chamber slides (Planegg, Germany).

Examination of mitochondrial morphology in MitoTracker Red CMXRos labeled cells. Cells were plated at 2500 cells/well for mNSC and 20 000 cells/well for hESC in 8-well Ibidi chamber slides and incubated for 24 h. They were treated with different concentrations of THS for 24 h after which MitoTracker Red CMXRos (Life Technologies, Grand Island, New York.) was added to each well at a final concentration of 300 nM and incubation continued for 30 min at 37°C. Cells were then washed with PBS and fixed with 4% paraformaldehyde at room temperature. Slides were covered with Vectashield mounting medium containing DAPI (Vector Laboratories Burlingame, California) and imaged using the Nikon Eclipse TI microscope (Nikon, Melville, New York). For all imaging experiments, fluorescence intensity was adjusted so that the group having the strongest fluorescence was imaged first at nonsaturating exposures, and the other groups were imaged using the same exposure parameters so that fluorescence could be compared across groups.

Quantification of the number of cells with different mitochondrial morphologies. MitoTracker Red labeled cells were evaluated for different mitochondrial morphologies (dots, tubes, networks, loops, and blobs). The number of cells having different types of mitochondria in the control and treatment groups was evaluated through visual inspection. For this, each cell was classified according to the predominant mitochondrial morphology. In some cells, there was more than 1 dominant morphology, so that cell fell into 2 categories. In total, 155–180 cells were analyzed in the different treatment groups. Interactomes demonstrating the distribution of different mitochondrial morphologies among cells in control and treated groups were prepared using the Cytoscape software (http://www.cytoscape.org/, Accessed June 3, 2016).

Analysis of mitochondria morphology. mNSC were treated and labeled with MitoTracker-Red dye as described above, then a combination of software tools was used to segment and classify mitochondrial shape as previously described (Zahedi *et al.*, 2015). CellProfiler software was used to segment the red fluorescence channel, and thresholding was performed using an adaption of Otsu's method. Morphological and intensity features were extracted for each segmented mitochondrion. These features were fed into a supervised learning algorithm written on the MATLAB platform. The software was trained with a mitochondrial library (approximately 100 samples of each morphological type). An exhaustive search was run to identify key features and combinations. The naïve Bayes classifier was then used to automatically categorize the mitochondria into dots, networks, loops, and blobs with 91% accuracy. These results were confirmed using the K-nearest neighbor classifier which gave 90% accuracy. Lastly, the segmented test dataset was analyzed by the classifier to determine the area of each morphological subpopulation. The area of each subpopulation was normalized to the total mitochondrial area of each cell and averaged across all cells within each treatment group.

Live cell imaging of mitochondrial fusion. A line of mNSC transfected with MitoTimer to visualize mitochondria were plated on chamber slides at 2500 cells/well and allowed to attach for 24 h after which they were treated with THS extract at 30% and 100% concentrations. After 24 h of treatment, the chamber slide was transferred to an incubation unit attached to a Nikon Eclipse Ti inverted microscope. Real time videos, which were obtained over 2 min of recording, were visually inspected for mitochondrial morphology transitions and fusion.

Evaluation of MMP. Cells treated with 30% and 100% concentrations of THS for 24 h and labeled with MitoTracker Red CMXRos were used to determine if THS affected MMP. MitoTracker Red CMXRos accumulation in live mitochondria is dependent on the MMP, and the probe is well retained after fixation. After treatment and labeling with MitoTracker Red, cells were fixed and imaged as described in the section on evaluation of mitochondrial morphology.

MitoTracker intensity analysis. A segmentation module was developed using Cl-Quant software (DR Vision, Seattle, Washington) to separate the mitochondria from the background. To compare mitochondrial intensities across groups, an intensity threshold of 160 was used, and only mitochondria with pixels above this threshold were counted. The number of mitochondria with intensities over 160 was averaged for each group. Each group contained 10 cells, and 3 experiments were performed.

ATP assay. Cells were plated at 10 000 cells/well in 12-well plates and were incubated for 24 h, after which various concentrations of THS were added. After 1, 4, and 24 h of incubation, cells were lysed at room temperature for 30 min using lysis buffer containing 10 mM Tris at pH 7.5, 100 mM NaCl, 1 mM EDTA, and 0.01% Triton X 100. Cells were centrifuged at 4°C for 5 min at 12 000 × g and supernatant was used to determine ATP concentrations. An ATP Determination Kit (Life Technologies) was used according to manufacturer's instructions to obtain luminescence readings using a Lucetta luminometer (Lonza, Portsmouth, New Hampshire). Twenty millimolar sodium azide treatment for 1 h was used as a positive control.

MitoSOX Red labeling for evaluation of superoxide production. Cells were plated at 2500 cells/well on chamber slides (Ibidi, Planegg, Germany) and incubated for 24 h at 37 °C. Cells were then incubated in 5 μM MitoSOX Red Mitochondrial Superoxide Indicator solution (Life Technologies) prepared in PBS for 15 min at 37 °C, after which medium was removed and cells were washed 2 times with PBS warmed to 37 °C. THS extracts were then added to the cells and images of live cells were acquired after 4 h of treatment using the Nikon Ti Eclipse microscope (Nikon).

Evaluation of mitochondrial protein oxidation using MitoTimer transfected cells. MitoTimer is a mutant of the red fluorescent protein dsRed that becomes localized in the mitochondria through a mitochondrial targeting sequence (cytochrome C oxidase subunit VIII). The fluorescence of the Timer protein changes from green to red with increased oxidation of the mitochondrial proteins (**Hernandez *et al.***, 2013). MitoTimer transfected cells (mNSC) were plated at 2500 cells/well on chamber slides (Ibidi,

Planegg, Germany) and incubated for 24 h at 37 °C. They were then treated with THS for 24 h and imaged using a Nikon Ti Eclipse microscope (Nikon). Images were analyzed using a protocol developed with CL-Quant software (DR Vision) to obtain ratios of red/green fluorescence.

Long-term exposure to THS. For long-term experiments spanning 15 and 30 days, cells were plated in 12-well plates at10 000 cell/well and allowed to attach for 24 h, after which THS was added. THS was replaced on alternate days. Cells were passaged on reaching 80% confluency and replated onto fresh 12-well plates at 10 000 cells/well in THS extract. On the second to last day of the treatment, cells were trypsinized and plated on chamber slides (Ibidi, Planegg, Germany) at 2500 cells/well for MitoTracker Red CMXRos staining. On the second to last day of each experiment, cells were also plated onto 24-well plates at 5000 cell/well for cell growth evaluation with a live cell imaging assay using Nikon BioStation CT (Nikon). THS was added at 10% and 30% concentrations, and cells were allowed to attach at 37°C for 24 h. After 24 h, plates were transferred to a Nikon BioStation CT incubator (Nikon) and imaged every 2 h for 46 h. For each well, data were collected from 5 different fields. Cell proliferation was analyzed in time-lapse images using video bioinformatics protocols created in CL Quant software (DR Vision) (Talbot *et al.*, 2014).

RT^2 PCR profiler array. mNSC were plated in 6-well plates at 30 000 cells/well and allowed to attach overnight at 37°C for 24 h. After 24 h, cells were treated with THS extracts at 100% concentration for 1, 4, or 24 h. RNA was isolated using the Qiagen RNAeasy plus mini kit (Qiagen, Velencia, California). RNA was checked for degradation using the Agilent 2100 Bioanalyzer, and only those samples having a RIN (RNA integrity number) of 7 or above were used for further processing. Four hundred nanograms of RNA from each sample were used to prepare cDNA using the Qiagen RT^2 First Strand Kit (Qiagen). cDNA was amplified through a PCR reaction using primers for beta-actin to make sure that the cDNA synthesis reaction has worked. Primer sequences used were as follows: 5′-TGGCATTGTTACCAAGTGGGACGAC-3′ (forward) and 5′-GGAACCGCTCGTTGCCAATAGTGAT-3′ (reverse).

The effect of THS on expression of 84 genes associated with mitochondrial function was evaluated using the Qiagen Mitochondria RT^2 Profiler Array. Reaction mixtures were prepared by mixing cDNA with Qiagen RT^2 SYBR Green FAST Mastermix according to manufacturer's protocol. Mixtures were loaded on to the array plate. RT-PCR was performed using the BIO-RAD CFX384 Real Time PCR detection system. Data were uploaded to the Qiagen Data Analysis Center for analysis and obtaining fold changes in gene expression.

Follow up PCR. The accuracy of the RT^2 Profiler Array was checked through RT-PCR for 2 genes that were downregulated on the array. Qiagen HotStarTaq Master Mix (Qiagen) was used to run PCR reactions with the BioRad Thermal Cycler (BioRad, Hercules, California). Primers used were as follows:

Fis1: 5′-AAAGTATGTGCGAGGGCTGT-3′ (forward) and 5′-ACA GCCAGTCCAATGAGTCC-3' (reverse); and *Aifm2*: 5′-GGTGAGC AACCTGGAGGAAC-3′ (forward) and 5′-GGTATCGGCACAGTCA CCAA-3′ (reverse). Lonza DNA FlashGels were run to separate PCR products which were imaged using a Lonza FlashGel imaging system (Lonza, Walkersville, Maryland).

Statistical analysis. GraphPad Prism software was used to perform statistical analyses. For fluorescent intensity data, the 30% THS and 100% THS groups were individually compared with the control group using a *t* test. For ATP data, which did not satisfy the assumptions of ANOVA, the nonparametric Kruskal-Wallis test was performed. ATP values for treatment and control groups were normalized to the total protein in each group and were transformed using the arcsine function before comparing treated and control groups. When significance was found, Dunn's *post hoc* test was used to isolate the significance to specific treatment groups. For MitoTimer experiments, the raw data from 30% to 100% THS-treated groups were compared with control groups using a *t* test. For area analysis following long-term exposure, 4 fields from 1 experiment were averaged. The area at the last time point was compared using a 1-way ANOVA. Dunnett's *post hoc* test was used to isolate the significance to specific treatment groups. RT^2 Profiler Array data were uploaded to the Qiagen data analysis center to obtain fold changes that were statistically significant.

RESULTS

Exposure and Extraction of THS From Terry Cloth

THS was extracted from terry cloth that had been exposed to cigarette smoke for 3 different lengths of time. All results, except those dealing with MMP during 24 h of treatment, were obtained with THS from terry cloth that had been exposed to 133 cigarettes over 11 months and aged for 15 months prior to extraction and testing. For the experiment dealing with MMP at 24 h, THS was extracted from terry cloth exposed to 11, 75, or 133 cigarettes over 4, 9, and 11 months, respectively. In all experiments, 100% refers to solutions obtained by extracting 0.125 g of fabric in 1 ml of culture medium, and 30% and 10% extracts were made by diluting the 100% extracts with culture medium. Based on analyses done previously (Bahl *et al.*, 2014), the nicotine concentration in extracts of terry cloth exposed to 133 cigarettes over 11 months was: (1) about 875 ng of nicotine/ml of culture medium for the 10% extracts; (2) 2.6 μg of nicotine/ml of culture medium for the 30% extracts, and (3) 8.75 μg of nicotine/ml of culture medium for the 100% extracts. While nicotine was not necessarily the active chemical in our assays, these concentrations of nicotine provide a basis for comparing data across THS studies and to levels of exposure once data on nicotine concentrations in the blood of human subjects exposed to THS becomes available.

THS Treatment Altered Mitochondrial Morphology

The morphology of mitochondria in control mNSC and cells treated 24 h with 30% and 100% THS extracts from 133 cigarettes was examined after labeling with MitoTracker Red CMXRos (Figs. 1A and B). Control mNSC had numerous mitochondria clustered around the nucleus (Figure 1A). Most mitochondria in control cells were categorized as small "dots" (Figs. 1A and B). In THS-treated mNSC, 4 morphologies of mitochondria were observed: dots, tubes/networks, loops, and blobs (Figs. 1A and B). While a few cells in the control group had multiple mitochondrial morphologies, most control cells had mainly dot mitochondria. In contrast, in the THS treatment groups, most cells had tube, network, loop, and blob mitochondria with fewer cells having dot mitochondria (Figure 1A). To demonstrate this difference, interactomes were constructed for the control and THS-treated groups (Figure 1C). Colored circles in the interactomes represent different mitochondrial morphologies, whereas the small white circles are individual cells. Lines connecting the cells to different circles represent the presence of

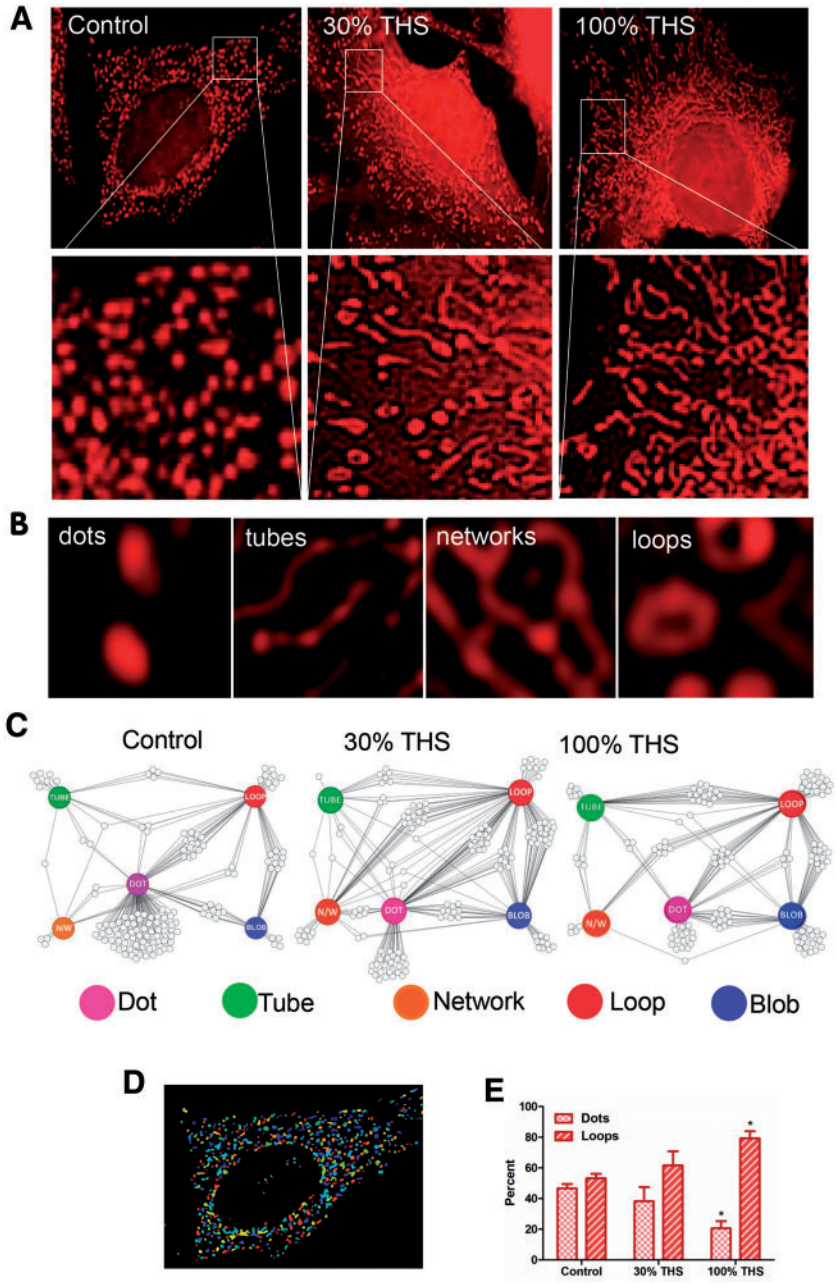

Fig. 1. Micrographs showing different mitochondrial morphologies in THS-treated mNSC. **A**, Mitochondrial morphologies in control and THS-treated groups. **B,** Examples of 4 mitochondrial morphologies present in mNSC. **C,** Interactomes showing distribution of different mitochondrial morphologies in cells from control and treatment groups. Each interactome represents 150 cells that were inspected visually. Hollow circles represent individual cells and colored circles or nodes represent morphological types. Connecting lines between hollow and colored circles represent the presence of multiple morphologies in a single cells. **D,** Example of a cell that has been segmented to quantify different morphological types of mitochondria. **E,** Percent of dot and loop mitochondria in control and treated cells. As THS concentration increased, there were fewer dots and more loops in treated cells than in the control. Each group is the mean ± SEM of 3 experiments. * = P< .05.

those mitochondrial morphologies in the cells. It is clear from the increased complexity of the treatment group interactomes that treated cells had fewer dot mitochondria and more of the other mitochondrial morphologies relative to the control (Figure 1C).

Mitochondria were segmented using Cell Profiler (Figure 1D), and the number of dot and loop mitochondria were compared in control and treated cells (Figure 1E). Treated groups had relatively fewer dots and more loops than controls. These differences were significant at the 100% THS concentration.

Changes in Mitochondrial Morphology Occurred Through Mitochondrial Fusion

To test the hypothesis that the changes in mitochondrial morphology observed in THS-treated cells were due to fusion of mitochondria, control and treated cells were transfected with MitoTimer, a protein targeted to the mitochondria, and videos were made of cells to observe their behavior over time. In both control and treated groups, mitochondria were constantly moving within cells. During movement, mitochondria in treated cells underwent fusion either with adjacent mitochondria or

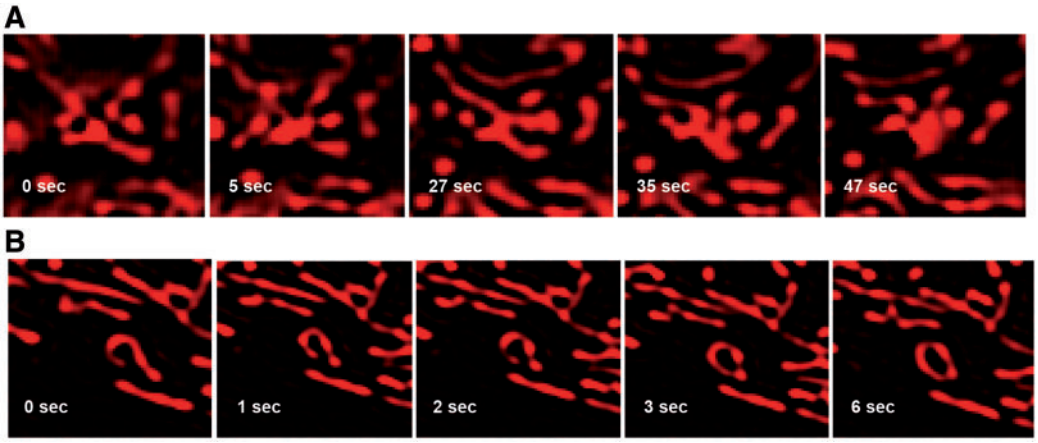

Fig. 2. Mitochondrial fusion. **A**, Filmstrip of MitoTimer transfected mNSC showing aggregation of dotted mitochondria to form blob-like mitochondria through fusion. **B**, Filmstrip of MitoTimer transfected mNSC showing the transition of a tubular mitochondrion into a loop though circularization of the tube and fusion of its ends.

with themselves as shown in Figures 2A and B. Dot mitochondria fused with each other to form blobs (Figure 2A) or tubes (not shown). Tubular mitochondria either fused with each other to form networks (not shown) or curled so that their ends fused to form loops (Figure 2B). These transitions occurred within seconds to minutes. While some mitochondrial fission occurred, mitochondrial fusion was dominant in THS-treated cells. These data support the hypothesis that THS treatment produced SIMH, as described previously in mouse embryonic fibroblasts exposed to various stressors (Tondera *et al.*, 2009)

THS Treatment Increased MMP and ATP Production in mNSC

SIMH was shown previously to increase ATP production (Tondera *et al.*, 2009). We hypothesized that THS would increase MMP) and ATP levels of treated cells. To test this, mNSC were treated with extracts from terry cloth that had been exposed to THS from 11, 75, or 133 cigarettes. After 24 h of treatment, cells were labeled with MitoTracker Red CMXRos, which accumulates in mitochondria in direct proportion to the MMP and is retained after fixation. All THS extracts increased the MMP of mNSC (Figs. 3A–C), as demonstrated by a dose-dependent increase of fluorescence in the treated groups. The increased fluorescence was greatest in cells treated with extracts from terry cloth exposed to 133 cigarettes. Cells treated with extracts from unexposed terry cloth had fluorescence intensity similar to that of cells incubated in culture medium (control cells). hESC showed a similar increase in fluorescence in the THS-treated groups (Supplementary Figure 1); however, these cells were not studied further as their mitochondria were difficult to resolve due to the compact nature of the hESC cytoplasm.

The number of mitochondria/cell that had a fluorescent intensity above 160 was quantified in NSC, and the 100% THS-treated group was significantly higher than the control (Figure 3D). Since an increase in MMP and SIMH are likely accompanied by increased ATP production, we incubated cells in 30% and 100% THS extracts for 24 h, then tested cell lysates for levels of ATP using a luminescence-based assay. ATP production increased in groups treated with both 30% and 100% THS. ATP in the 100% concentration was significantly higher than in the control (Figure 3E).

THS Increased ROS Production and Oxidation of Mitochondrial Proteins

To test the hypothesis that increased MMP and ATP production would be accompanied by an increase in ROS, cells were treated for 6 h with THS extract then incubated in MitoSOX Red, which fluoresces in the presence of superoxide anions (Figure 4A). Approximately 30% and 100% THS extracts increased superoxide anion production as demonstrated by MitoSOX Red labeling. MitoSOX Red fluorescence was concentrated in the mitochondria of most THS-treated cells, whereas mitochondria in the control group did not show MitoSOX Red fluorescence (Figure 4A).

Oxidative stress was further evaluated using MitoTimer transfected mNSC. MitoTimer is a mutant of red fluorescent protein dsRed which is inserted into mitochondria through a targeting sequence, derived from cytochrome c oxidase subunit VIII, that is used to deliver proteins to the mitochondria (Hernandez *et al.*, 2013). Newly synthesized MitoTimer protein emits green fluorescence, which changes to red upon protein aging and oxidative damage. An increase in the red/green fluorescence ratio is an indicator of accumulated oxidation in mitochondrial proteins (Hernandez *et al.*, 2013). mNSC exposed to THS for 24 h were imaged using a fluorescence microscope, and both the 30% and 100% THS extracts caused an increase in the red/green fluorescence ratio when compared to the control cells (Figure 4B). Quantification of the red/green fluorescence ratio using CL-Quant software confirmed that oxidation of the MitoTimer protein increased during exposure to THS extract (Figure 4C).

Long-Term Treatment of mNSC With THS Caused a Reduction in MMP and Altered Proliferation Rate

To test the hypothesis that prolonged exposure to THS leads to deceased mitochondrial function and cell growth, mNSC were treated with THS extracts at 10% and 30% concentrations for 15 or 30 days, then labeled with MitoTracker Red and imaged. Results from 1 of 2 representative experiments are shown in Figure 5. After 15 days, MitoTracker Red fluorescence was higher in the THS-treated groups (Figure 5A), indicating that MMP can remain elevated for over 2 weeks in THS-treated cells. By 30 days of exposure, fluorescence in the treated groups was less than in the control (Figure 5B). The number of mitochondria/cell with a fluorescent intensity above 160 was increased after 15 days (Figure 5C), but reduced after 30 days of treatment (Figure 5D). This shows that MMP can be compromised by prolonged exposure (30 days) to THS.

To determine if cell growth rate was affected by prolonged exposure to THS, cells were trypsinized and replated at 5000

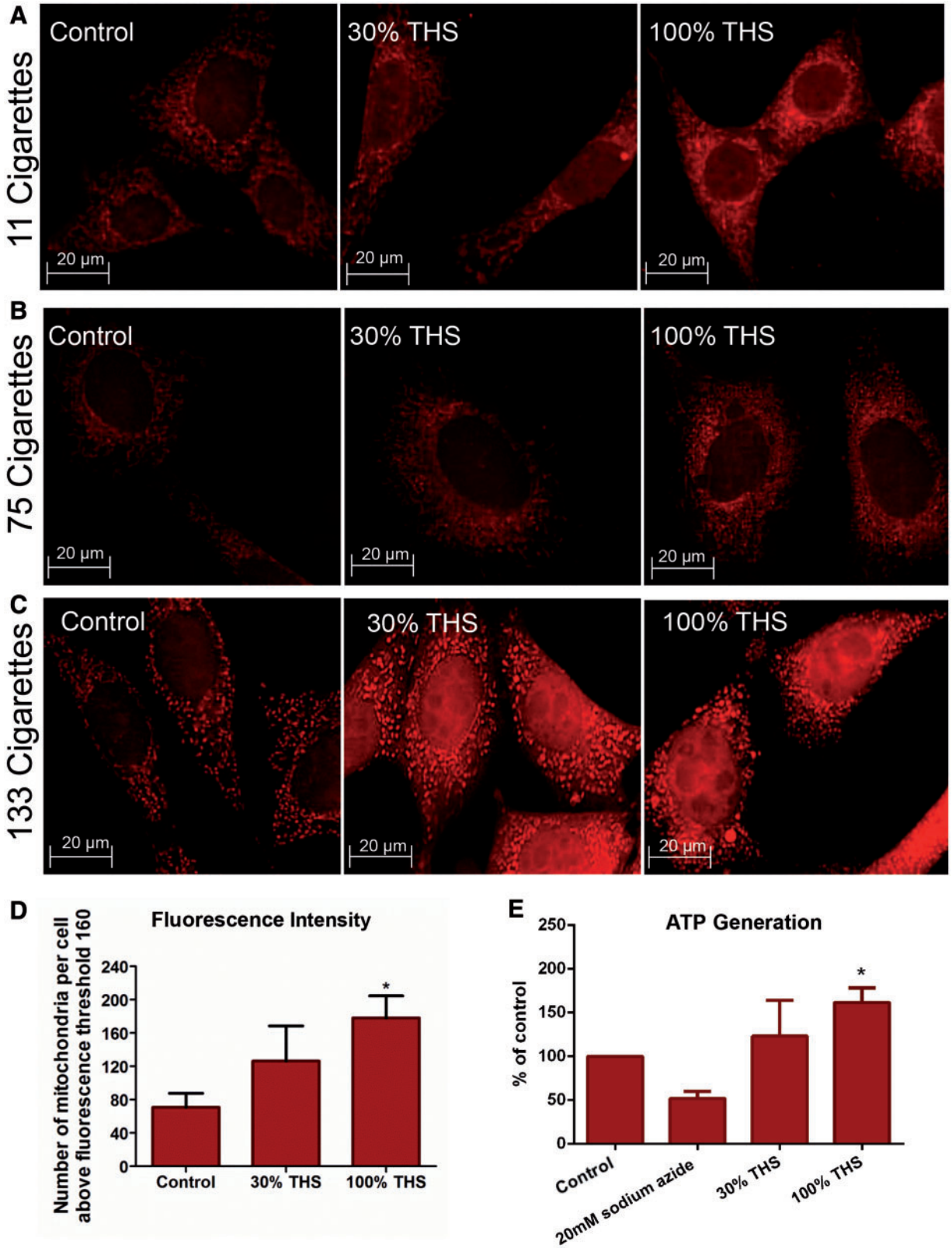

Fig. 3. THS treatment increased MMP in mNSC as seen with labeling and ATP levels. Control and THS-treated cells were labeled with MitoTracker Red CMX Ros which accumulates in mitochondria in proportion to their MMP. **A,** mNSC cells treated with THS extract from terry cloth exposed to 11 cigarettes over 4 months. **B,** mNSC treated with THS extract from terry cloth exposed to 75 cigarettes over 9 months. **C,** mNSC treated with THS from terry cloth exposed to 133 cigarettes over 11 months and aged for 15 months. **D**, Graph showing percentage of mitochondria/per cell with fluorescent intensity above 160 in control cells and cells treated with 30% and 100% THS from fabric exposed to 133 cigarettes. Each bar is a mean ± SEM of 3 experiments. **E,** Graph showing ATP generation in control and treated cells. Each bar shows mean ± SEM of 3 experiments. * = $P < .05$.

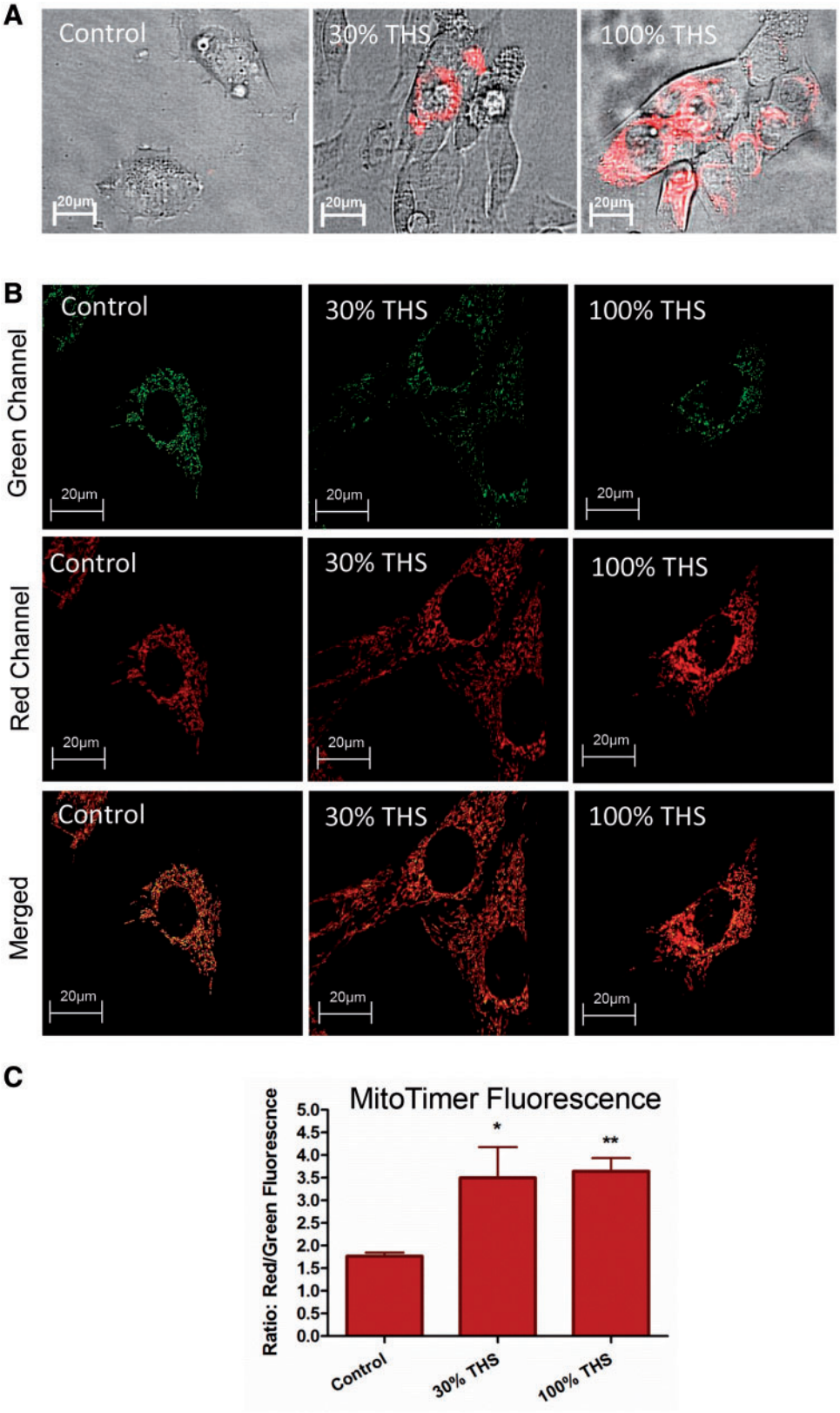

Fig. 4. THS increased oxidative stress. **A,** Micrographs showing control and THS treated mNSC labeled with MitoSOX Red, which fluoresces when binding superoxide anion. Fluorescent images are superimposed on phase images to demonstrate the localization of MitoSOX labeling in mitochondria clustered around the nuclei in treated cells. **B,** Micrographs showing mNSC transfected with MitoTimer. Red and green fluorescent images are shown individually as well as superimposed. **C,** Ratio of MitoTimer red/green fluorescence in control and THS-treated cells. Each bar shows mean ± SEM of 3 experiments. 30% and 100% THS. * = $P < .05$; ** = $.001 < P < .01$.

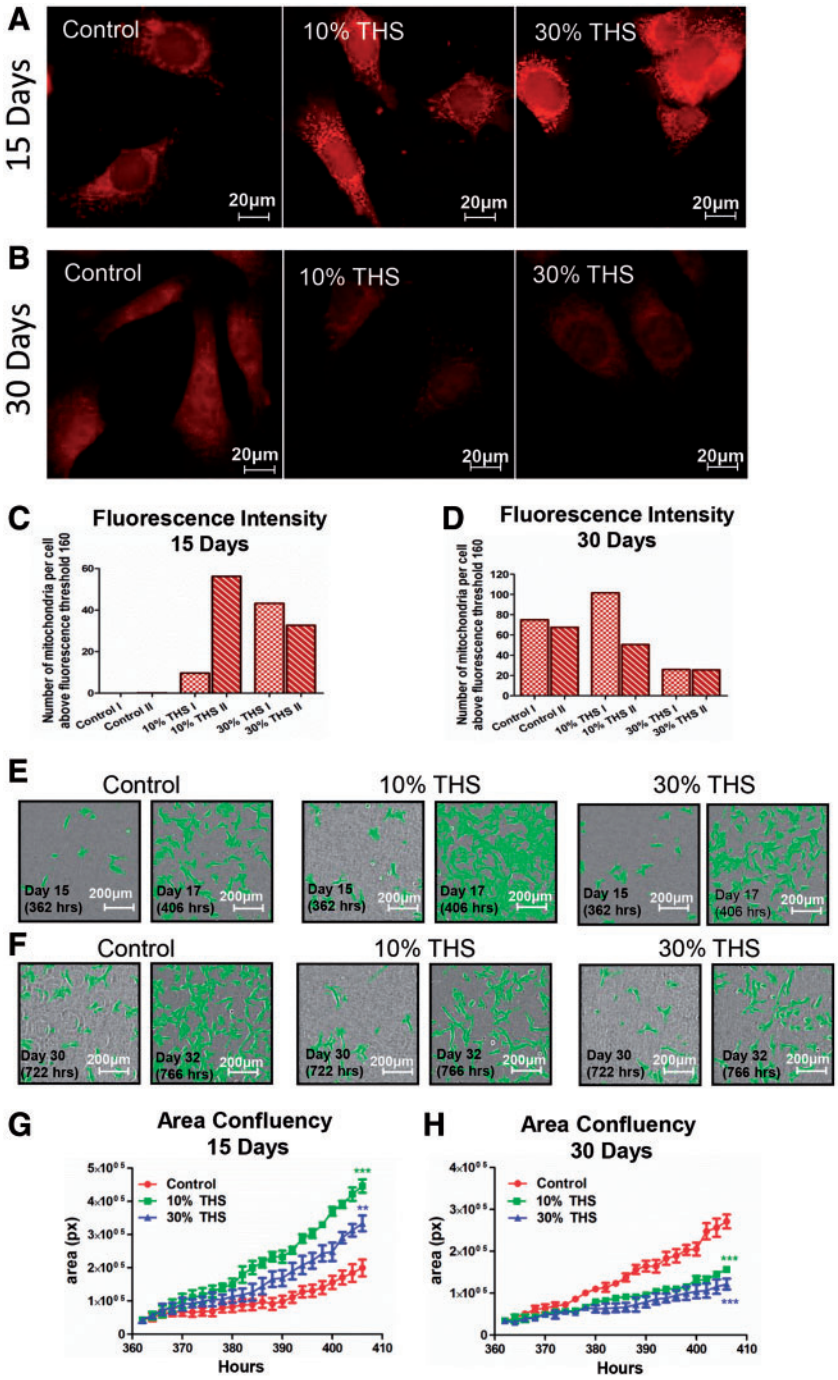

Fig. 5. MMP and cell growth rate decreased after long-term THS exposure. **A,** Micrographs showing control and treated cells labeled with MitoTracker Red CMXRos after 15 days of THS treatment. **B,** Micrographs showing control and treated cell labeled with MitoTracker Red CMXRos after 30 days of treatment. **C,** Graph showing number of mitochondria/cell with a fluorescent intensity above 160 in 2 individual 15 day experiments. **D,** Graph showing number of mitochondria/cell with a fluorescent intensity above 160 in 2 individual 30 day experiments. **E,** Segmented micrographs showing density of mNSC after 15–17 days of treatment. **F,** Segmented micrographs showing density of mNSC after 30–32 days of treatment. **G,** Graph showing cell proliferation data from 1 of 2 representative experiments in which cells were treated with THS for 17 days. **H,** Graph showing cell proliferation data from 1 of 2 representative experiments in which cells were treated with THS for 32 days. In G and H, each point is the mean ± SEM of 4 different frames. ** = .001 < P < .01; *** = P < .001.

cells/well in 24-well plates on day 14 of treatment in the 15 day experiment and on day 29 of treatment in the 30 day experiment. Cells were then imaged live for 46 h starting on day 15 and day 30 of the treatments, respectively. In the 15 day experiment cell confluency was higher in the THS-treated groups when compared with the control group, indicating increased proliferation (Figure 5E). In the 30 day experiment, THS-treated groups had fewer cells than control groups indicating decreased proliferation (Figure 5F). Consecutive frames were checked visually for presence of dead cells, but no dead cells were found. Area confluency was quantified using CL-Quant. After 15 days of treatment, the proliferation rate was significantly higher for

10% and 30% THS-treated groups (Figure 5G), whereas after 30 days, the proliferation rate was significantly lower in the 10% and 30% THS treatment groups (Figure 5H).

THS Altered the Transcriptional Profile of Genes Associated With Mitochondrial Function

Gene expression was evaluated using Qiagen RT^2 Mitochondria Profiler Arrays after 1, 4, and 24 h of exposure to THS. After 1 h of treatment, expression of the mitochondrial membrane transporter *Slc25a25* was decreased by 2.14-fold, whereas expression of *Ucp4* and *Taz* increased by over 2-fold (Figure 6A). At 4 h of treatment, 25 genes associated with mitochondrial function showed a 2-fold or greater reduction in expression. These included *Fis1, Aifm2, Bbc3, Bid, Tspo, Ucp2, Ucp4*, and *Ucp5* (Figure 6B), and transporters from the SLC25A and TIMM families. PCR was used to confirm the array results for *Fis1 and Aifm2*, two of the genes that were affected by treatment (Figure 6C). The relative number of affected genes in different functional groups is shown in Figure 6D. The genes that play a role in SIMH and their functions are given in Figure 6E. A complete list of the affected genes and their functions is given in Table 1. No significant alterations in gene expression were observed at 24 h of treatment relative to the 24 h control.

DISCUSSION

Mitochondria are exquisitely sensitive monitors of cell health and respond in multiple ways to environmental stress (Meyer *et al.*, 2013). In this study, THS extracts, which had no effect in the MTT assay, had profound morphological and physiological effects on mitochondria leading to the results summarized in Figure 7. The effects on mitochondria included the formation of tube/network, loop, and blob mitochondria from dot mitochondria. These morphological changes were brought about by mitochondrial fusion and are consistent with SIMH. SIMH in mNSC was accompanied by increased MMP (also observed in hESC) with increased ATP production, increased levels of superoxide, and increased oxidation of mitochondrial proteins. Alterations in gene expression in treated cells were consistent with reduced mitochondrial fission and protection of cells from apoptosis. Extended exposure to THS for 15 days led to an increase in both MMP and cell proliferation, whereas both of these processes were decreased by treatment for 30 days. We show for the first time that sublethal doses of THS can cause SIMH and alter mitochondrial function in a manner that could protect cells in the short term, but lead to cell loss/death with chronic exposure.

While mitochondria often fragment in response to external stress (Leboucher *et al.*, 2012), Tondera *et al.* (2009) reported that mitochondria in mouse embryonic fibroblasts undergo SIMH following exposure to certain types of environmental stress including treatment with actinomycin D and UV radiation (Tondera *et al.*, 2009). It was previously reported that 10% and 12.5% solutions of cigarette smoke extract (smoke from 4 cigarettes bubbled through a 50 ml solution was considered 100%) caused fragmentation of mitochondria in BEAS-2B cells, but at the 1% concentration there was branching and hyperfusion of mitochondria (Hoffmann *et al.*, 2013). Alveolar epithelial cells also undergo mitochondrial hyperfusion when treated with nontoxic doses of 25% cigarette smoke extracts (where smoke from 6 cigarettes was bubbled through 100 ml of medium and served as the 100%) (Ballweg *et al.*, 2014). Our results demonstrate that similar effects on mitochondrial fusion are produced by THS from 133 cigarettes collected over 11 months. These effects of THS are not lethal in short-term experiments, as the batch of THS that we used was not cytotoxic in the MTT assay and did not affect the morphology and motility of mNSC. However, in our experiments, THS not only caused SIMH, but also increased MMP, ATP, ROS, and mitochondrial protein oxidation and altered of the expression of genes involved in mitochondrial function. These latter effects were not previously described in the studies with cigarette smoke.

SIMH is likely a protective response to stress that allows healthy mitochondria to rescue those that are damaged (van der Bliek, 2009) and enables treated cells to produce sufficient ATP to combat stress (Tondera *et al.*, 2009). In addition, SIMH is likely to protect mitochondria from autophagosomal degradation due to the large size of the hyperfused mitochondria (Gomes *et al.*, 2011). SIMH occurs when the balance between fusion and fission is tipped in favor of fusion by either an increase in level of profusion genes, such as *Mitofusin-1* (Tondera *et al.*, 2009), or a decrease in profission genes, such as *Fis1* (this study). Although we did not observe an increase in *Mitofusin-1* expression, we did find that expression of *Fis1*, was reduced. This could create an imbalance between *Fis1* and *Mitofusin* 1 and tip the balance toward fusion, as was seen in our study. In a related study, a decrease in *DRP1* expression, another gene responsible for fission, was observed during mitochondrial hyperfusion (Gomes *et al.*, 2011). Our data and that of (Tondera *et al.*, 2009) suggest that different mechanisms exist for regulating SIMH, and these mechanisms may vary with cell type and/or the source of the stress.

Highly networked and tubular mitochondria have also been reported to play a protective role against cell death in conditions of nutrient starvation (Rambold *et al.*, 2011). The network/tubular mitochondria observed in our study may protect against THS-induced stress, which is further supported by the decreased expression of genes associated with apoptosis. Apoptosis inducing factor-mitochondrial 2 (*Aifm2*), Bcl binding component 3 (*Bbc3*), and BH3 interacting domain death agonist (Bid), which are all involved in apoptosis (Han *et al.*, 2001; Joza *et al.*, 2001; Li *et al.*, 1998), were down regulated in cells treated with THS. Translocator protein (*Tspo*), which also showed decreased expression, may be involved in preventing apoptosis, as its down regulation leads to reduced mitochondrial outer membrane permeablization, thus restricting the release of pro-apoptotic factors, such as apoptosis-inducing factor (Gatliff and Campanella, 2012). In addition, decreased expression of *Fis1* protects cells from apoptosis (Lee *et al.*, 2004), perhaps by favoring hyperfusion, which occurred in our study. There were no significant changes in gene expression at 24 h of treatment. This may be because changes in gene expression that occur early during treatment have long lasting effects, or because changes in gene expression are cyclic, or because the 84 genes on our arrays did not have altered expression at 24 h.

SIMH was accompanied by increases in MMP, ATP, and mitochondrial ROS levels (MitoSOX Red). Our RNA profiling data showed that 3 genes associated with decreasing MMP (*Slc25a8/Ucp2, Slc25a27/Ucp4*, and *Slc25a14/Ucp5*) were down regulated in THS-treated cells, which may have contributed to the MMP increase that we observed. *UCP* 2, 3, and 4 are members of the solute carrier family *SLC25A* and cause uncoupling of mitochondrial oxidative phosphorylation, thus diminishing oxidative stress in cells (Brand and Esteves, 2005; Ramsden *et al.*, 2012) . *UCP2* in human pluripotent stem cells regulates energy metabolism by preventing oxidative phosphorylation and promoting glycolysis, which is the primary energy production pathway in stem cells (Zhang *et al.*, 2011). Since neural stem cells also rely mainly on glycolysis (Candelario *et al.*, 2013),

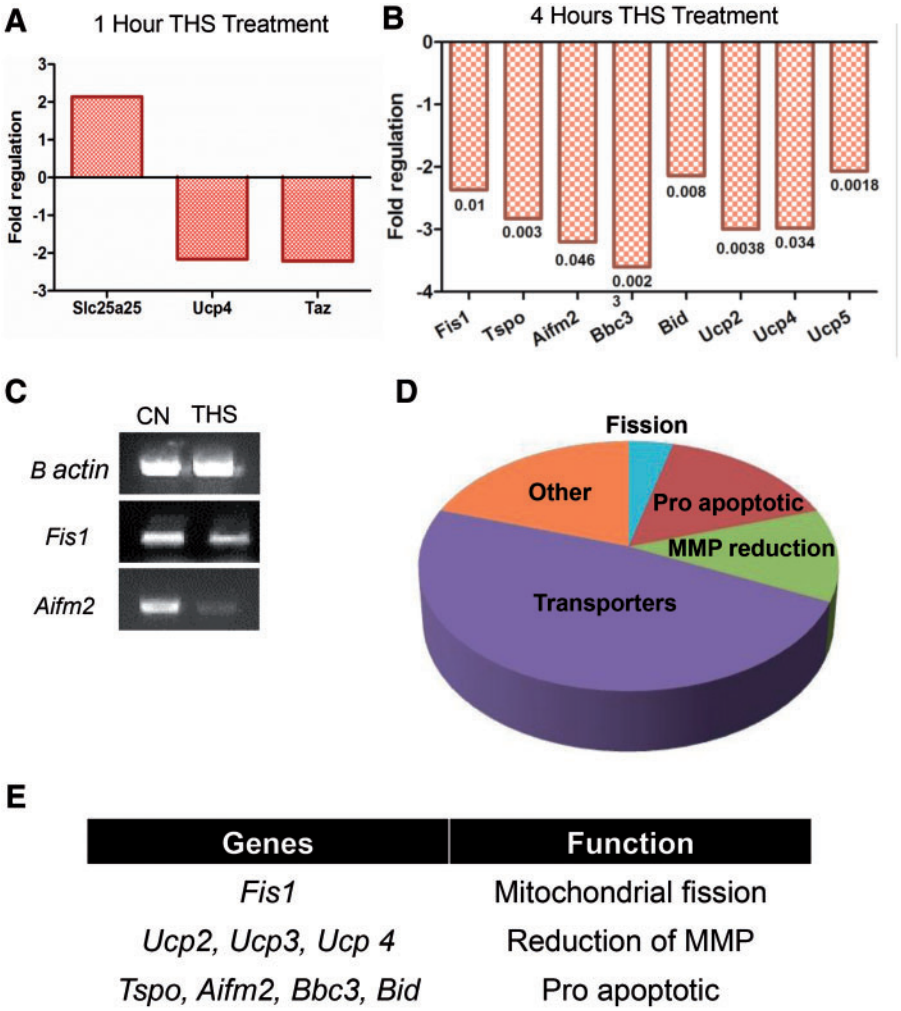

E

Genes	Function
Fis1	Mitochondrial fission
Ucp2, Ucp3, Ucp 4	Reduction of MMP
Tspo, Aifm2, Bbc3, Bid	Pro apoptotic

Fig. 6. THS caused significant changes in expression of genes associated with mitochondrial function. **A,** Changes in gene expression detected with RT^2 Profiler Arrays after 1 h of treatment with THS. Each bar is an average of 2 experiments. **B,** Changes in gene expression detected in RT^2 Profiler Arrays after 4 h of treatment with THS. Each column represents the average of 3 experiments. The numbers below each column represent the *P* value for fold change versus the control. **C,** RT-PCR products observed with gel electrophoresis to confirm the array data. β-actin was used as the housekeeping (loading) control. **D,** Pie chart showing the relative abundance of genes related to mitochondrial functions that were significantly down regulated by 4 h of THS treatment. **E,** Table summarizing the functions of genes with altered expression that may play a role in SIMH.

decreased expression of *Ucp2* by THS treatment could facilitate increased oxidative phosphorylation, which is supported by increased MMP and ATP production and could lead to the increased ROS that we observed. Increased oxidative stress is believed to drive stem cell differentiation (Rafalski and Brunet, 2011), but mNSCs treated with THS did not differentiate as is indicated by their stem cell-like morphology even after 30 days of exposure to THS. MMP, which was elevated through 15 days of exposure to THS, was accompanied by an increase in cell proliferation. At 15 days of exposure, the cells seemed healthy as indicated by normal morphology and motility. It is likely that the ATP being generated during SIMH is used to support increased proliferation, which may indicate that oxidative stress during SIMH drives proliferation instead of differentiation, although this idea requires further work for confirmation. After 30 days of exposure, cells had a decreased MMP accompanied by a decrease in proliferation, indicating that at some point, cells succumb to the stressor, and may eventually die.

Increased MMP and ATP production were likely consequences of SIMH, which increased ATP in mouse embryonic fibroblast exposed to UV light or actinomycin (Tondera *et al.*, 2009). Networked mitochondria, similar to those found in SIMH, have been associated with increased oxidative phosphorylation in cancer cells (Rossignol *et al.*, 2004). Certain mitochondrial morphologies, like blobs, are associated with increased ROS production in BEAS 2B cells (a line from normal human bronchial epithelium) (Ahmad *et al.*, 2013) and are similar to the results of our study. Our hypothesis that the increase in mitochondrial ROS would lead to oxidation of mitochondrial proteins was confirmed by the color shift in the MitoTimer protein to predominantly red fluorescence, which is indicative of protein oxidation in the THS-treated group. Although not evaluated in this study, increased ROS generation can cause DNA and membrane damage in cells (Squier, 2001; Stark, 2005; Waris and Ahsan, 2006) and eventually in conjunction with protein damage can lead to adverse health outcomes, including carcinogenesis and neurodegenerative diseases (Uttara *et al.*, 2009; Ziech, *et al.*, 2011).

The THS exposed terry cloth used in most of our assays was aged at room temperature for 15 months prior to extraction. During aging, it is likely that the volatile organic chemicals

TABLE 1. Genes With Decreased Expression in Response to THS Exposure for 4 h

Gene	FoldRegulation	*P* Value	Function
Fis1	−2.36	0.011	Mitochondrial fission
Tspo (18 kDa translocator protein)	−2.8	0.004	Increases mitochondrial membrane permeability
Aifm2 (apoptosis inducing factor – mitochondrial 2)	−3.2	0.046	Pro apoptotic
Bbc3 (Bcl binding component 3)	−3.6	0.002	Pro apoptotic
Bid (BH3 interacting domain death agonist)	−2.14	0.008	Mediates apoptosis and mitochondrial damage
Msto1	−2.5	0.001	Mitochondrial restructuring
Sls25a8/Ucp2 (uncoupling protein 2)	−2.99	0.004	Prevents OXPHIOs and promoted glycolysis
Taz (Tafazzin)	−4.8	0.0013	Acylation of cardiolipin
Dnajc19/Hsp40	−2.11	0.004	Associated with prohibitins that play a role in cardiolipin acylation
Cp2 (carnitine acyltransferase)	−3.2	0.006	Involved in fatty acid metabolism
Aip (aryl hydrocarbon receptor interacting protein)	−2.13	0.0014	Aryl hydrocarbon activated transcription factor regulating xenobiotic metabolizing enzymes
Mipep (mitochondrial intermediate peptidase)	−2.09	0.005	Maturation of proteins entering the mitochondria
Timm10b (Mitochondrial Import Inner Membrane Translocase Subunit Tim9 B)	−2	0.01	Import and insertion of membrane protein into mitochondrial membrane
Timm17b (Mitochondrial Import Inner Membrane Translocase Subunit Tim17-B)	−2.89	0.0014	Transport of mitochondrial proteins from cytosol in to mitochondria
Timm22	−2.32	0.0008	
Immp21	−2.71	0.02	
Slc25a1 (Solute Carrier Family 25)	−2.29	0.018	Citrate transport across mitochondrial inner membrane
Slc25a14/Ucp5	−2.06	0.0018	Reduction of mitochondrial membrane potential
Slc25a15	−2.29	0.0009	Ornithine transport from cytosol to mitochondria
Slc25a16	−2.38	0.0009	Molecular exchange between cytosol and mitochondria
Slc25a17	−2.53	0.0016	Molecular exchange between cytosol and mitochondria
Slc25a19	−2.82	0.0009	Transport of thiamine pyrophosphate into mitochondria
Slc25a20	−2.46	0.008	Transport of acylcarnitine into mitochondrial matrix for oxidation by the fatty acid oxidation pathway
Slc25a23	−3.07	0.01	Calcium dependent mitochondrial solute carrier
Slc25a27/Ucp4	−2.98	0.034	Lowering of mitochondrial membrane potential

(VOC) present in the fabric were lost and that the mitochondrial effects we observed were caused by nonvolatile or semivolatile chemicals that are soluble in aqueous media (Bahl *et al.*, 2016b). The main routes of exposure for the chemicals in THS extracts would be dermal and inhalation for all age groups plus ingestion for toddlers and infants. Exposure to THS through ingestion carries potentially higher risks as THS chemicals can readily dissolve in saliva and intake through ingestion may be much higher than through the skin. Even though the THS chemicals are diluted in saliva, a toddler mouthing a THS contaminated fabric for a long time could potentially ingest enough THS to affect mitochondrial health in exposed cells. We previously measured the concentrations of nicotine, nicotine-related alkaloids, and tobacco-specific nitrosamines (TSNA) extracted from the terry cloth used in this study (Bahl *et al.*, 2014). These data showed that a 12 kg toddler mouthing 5 g of fabric containing THS from 133 cigarettes would be exposed to 529 μg of nicotine/day and 2.2 μg of TSNAs/day. These intake values would be less than that received by an active smoker but higher than respiratory exposure in passive smokers (6.8× higher for nicotine and 16 times higher for TSNAs). These values are based on THS from only 133 cigarettes and therefore are very low compared to most THS environments. Although we do not yet know which chemical(s) in THS cause SIMH, the above data with nicotine and TSNAs show that fabrics retain THS chemicals for long periods of time and that the concentrations of retained THS chemicals are high enough to be of concern. Because mitochondrial toxicity was extracted in aqueous culture medium, remediation by washing THS exposed fabrics may help decrease its toxicity to mitochondria.

It is important to emphasize that when cells were exposed to THS for 30 days, the 10% concentration caused a reduction of MMP and decreased cell proliferation indicating that doses of THS that do not immediately kill cells can adversely impact mitochondrial health and cell proliferation during prolonged exposure (the nicotine concentration in 10% extracts was about 850 ng/ml based on data in Bahl *et al.*, 2014). Moreover, infants and children exposed to THS environments are likely to receive a higher dose/kg of body weight than adults. THS-induced mitochondrial stress and decreased proliferation of neural stem cells over time may adversely affect brain development in infants and children, since some THS chemicals such as nicotine are readily transferred across the blood brain barrier (Mazzone *et al.*, 2010). However, this suggestion requires further investigation using animals and human subjects. Also noteworthy, in our study, a very low number of cigarettes was used to generate THS, but in a real-life scenario, THS deposition could occur for years resulting in exposure to much higher doses of THS than used in the current study.

CONCLUSIONS

Our data demonstrate that THS from relatively few cigarettes can produce a stress response in mitochondria and alter the transcriptional profile of genes involved in mitochondrial function, which in turn affect mitochondria and cellular health. Our findings support the idea that SIMH produced by THS at levels that do not rapidly kill cells is a prosurvival mechanism that protects cells from undergoing apoptosis, while prolonged exposure to THS decreases mitochondrial MMP and cell proliferation, and likely leads to cell death. The most important conclusion from this study is that even though a low dose of THS may

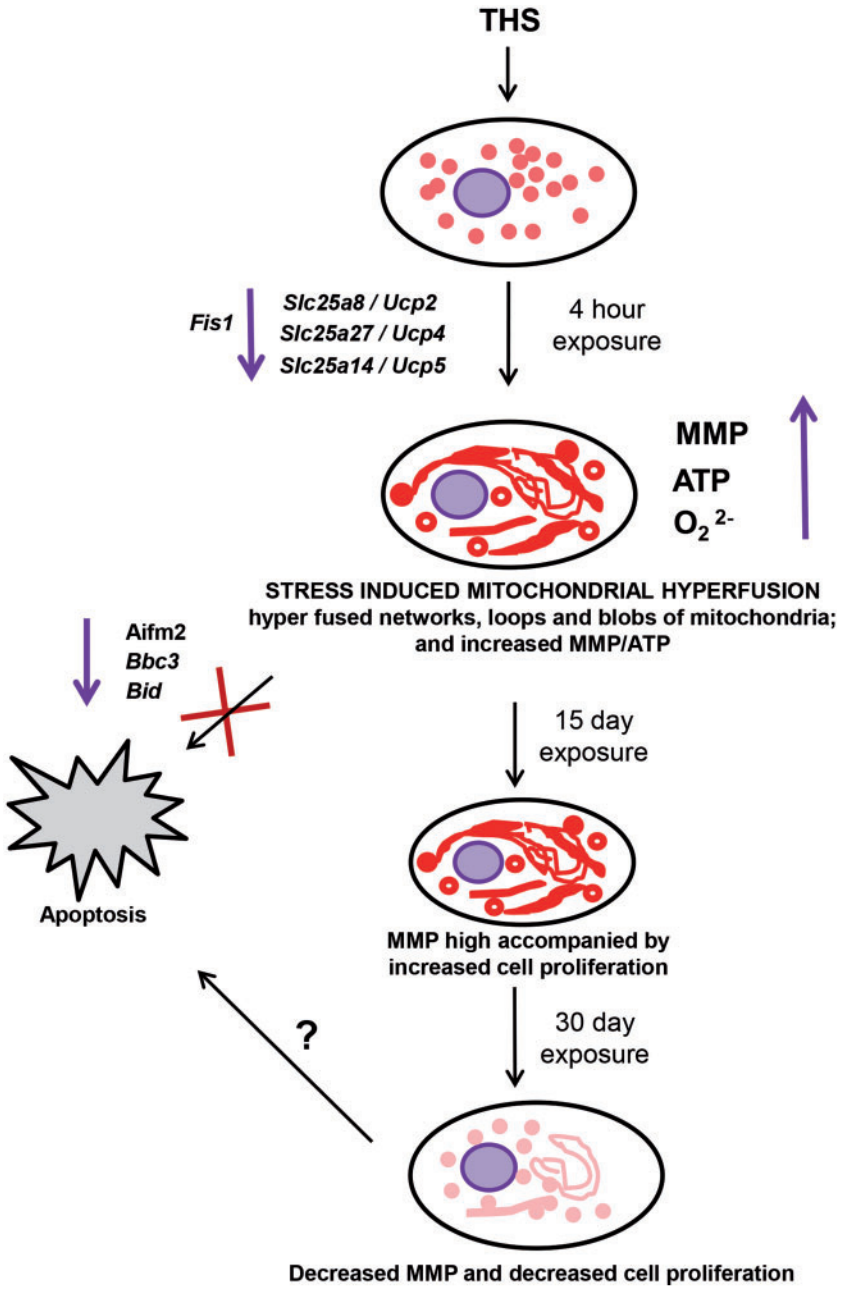

Fig. 7. Schematic summary of the effects of THS on mitochondria and cell health. Short-term exposure of mNSC to THS caused SIMH accompanied by increased MMP, ATP, superoxide anion, and oxidation of MitoTimer. SIMH is likely a prosurvival mechanism mediated by decreased expression of *Fis1* and proapoptotic genes. After long-term exposure up to 15 days, the cells still had a high MMP, but by 30 days of exposure, both MMP and cell proliferation decreased. Failure to survive THS exposure likely leads to apoptosis.

not directly kill cells, it induces a stressed state that compromise cellular function, survival and proliferation, and in turn could adversely affect the health of an exposed individual. Our data could be useful to agencies that regulate indoor smoking and may help parents make informed decisions regarding exposure of their children to THS.

SUPPLEMENTARY DATA

Supplementary data are available online at http://toxsci.oxfordjournals.org/.

FUNDING

Research carried at UCR was funded by grants from the Tobacco-Related Disease Research Program of California (Nos 20PT-0184 and 24RT-0037). V.B. was supported by a California Tobacco Related Disease Research Program Dissertation Research Award (No. 22DT-0002). The indoor exposure experiment at UCSF was supported by the California Tobacco Related Disease Research Program (No. 21ST-011). Funding sources were not involved in the design, collection, analysis, or interpretation of the data.

REFERENCES

Ahmad, T., Aggarwal, K., Pattnaik, B., Mukherjee, S., Sethi, T., Tiwari, B. K., and Agrawal, A. (2013). Computational classification of mitochondrial shapes reflects stress and redox state. *Cell Death Dis.* **44**, e461.

Bahl, V., Jacob, P., Havel, C., Schick, S. F., and Talbot, P. (2014). Thirdhand cigarette smoke: Factors affecting exposure and remediation. *PLoS One* **9**, e108258.

Bahl, V., Shim, H. J., Jacob, P., III, Dias, K., Schick, S. F., and Talbot, P. (2016a). Thirdhand smoke: Chemical dynamics, cytotoxicity, and genotoxicity in outdoor and indoor environments. *Toxicol InVitro*. **32**, 220–231.

Bahl, V., Weng, N. J., Schick, S. F., Sleiman, M., Whitehead, J., Ibarra, A., and Talbot, P. (2016b). Cytotoxicity of thirdhand smoke and identification of acrolein as a volatile thirdhand smoke chemical that inhibits cell proliferation. *Toxicol. Sci.* **150**, 234–246.

Ballweg, K., Mutze, K., Konigshoff, M., Eickelberg, O., and Meiners, S. (2014). Cigarette smoke extract affects mitochondrial function in alveolar epithelial cells. *AJP*. **307**, L895–L907.

Behar, R. Z., Bahl, V., Wang, Y., Weng, J. H., Lin, S. C., and Talbot, P. (2012a). Adaptation of stem cells to 96-well plate assays: Use of human embryonic and mouse neural stem cells in the MTT assay. *Curr. Protoc. Stem Cell Biol.* Chapter 1:Unit 1C.13.

Behar, R. Z., Bahl, V., Wang, Y., Lin, S., Xu, N., Davis, B., and Talbot, P. (2012b). A method for rapid dose–response screening of environmental chemicals using human embryonic stem cells. *J. Pharmacol. Toxicol. Methods* **66**, 238–245.

Brand, M. D., and Esteves, T. C. (2005). Physiological functions of the mitochondrial uncoupling proteins UCP2 and UCP3. *Cell Metab*. **22**, 85–93.

Candelario, K. M., Shuttleworth, C. W., and Cunningham, L. A. (2013). Neural stem/progenitor cells display a low requirement for oxidative metabolism independent of hypoxia inducible factor-1alpha expression. *J. Neurochem*. **125**, 420–429.

Chen, H., and Chan, D. C. (2009). Mitochondrial dynamics-fusion, fission, movement, and mitophagy-in neurodegenerative diseases. *Hum. Mol. Genet*. **18**, R169–R176.

Chen, H., Vermulst, M., Wang, Y. E., Chomyn, A., Prolla, T. A., McCaffery, J. M., and Chan, D. C. (2010). Mitochondrial fusion is required for mtDNA stability in skeletal muscle and tolerance of mtDNA mutations. *Cell* **141**, 280–289.

Collins, Y., Chouchani, E., James, A., Menger, K., Cochemé, H., and Murphy, M. (2012). Mitochondrial redox signalling at a glance. *J Cell Sci.* **125**, 801–806.

Detmer, S. A., and Chan, D. C. (2007). Functions and dysfunctions of mitochondrial dynamics. *Nat. Rev. Mol. Cell Biol.* **88**, 870–879.

Dwyer, J. B., McQuown, S. C., and Leslie, F. M. (2009). The dynamic effects of nicotine on the developing brain. *Pharmacol. Ther.* **122**, 125–139.

Ernest, M., Moolchan, E. T., and Robinson, M. l. (2001). Behavioral consequences of prenatal exposure to nicotine. *J. Am. Acad. Child Adolesc. Psychiatry* **40**, 630–641.

Gatliff, J., and Campanella, M. (2012). The 18 kDa translocator protein (TSPO): A new perspective in mitochondrial biology. *Curr. Mol. Med*. **12**, 356–368.

Gerbitz, K. D., Gempel, K., and Brdiczka, D. (1996). Mitochondria and diabetes: Genetic, biochemical, and clinical implications of the cellular energy circuit. *Diabetes* **45**, 113–126.

Gomes, L. C., Di Benedetto, G., and Scorrano, L. (2011). During autophagy mitochondria elongate, are spared from degradation and sustain cell viability. *Nat. Cell Biol.* **13**, 589–598.

Han, J., Flemington, C., Houghton, A. B., Gu, Z., Zambetti, G. P., Lutz, R. J., and Chittenden, T. (2001). Expression of bbc3, a pro-apoptotic BH3-only gene, is regulated by diverse cell death and survival signals. *Proc. Natl. Acad. Sci. U S A.* **98**, 11318–11323.

Hang, B., Sarker, A. H., Havel, C., Saha, S., Hazra, T. K., Schick, S., and Gundel, L. A. (2013). Thirdhand smoke causes DNA damage in human cells. *Mutagenesis* **28**, 381–391.

Hara, H., Araya, J., Ito, S., Kobayashi, K., Takasaka, N., Yoshii, Y. and Kuwano, K. (2013). Mitochondrial fragmentation in cigarette smoke-induced bronchial epithelial cell senescence. *Am. J. Physiol. Lung Cell. Mol. Physiol.* **305**, L737–L746.

Hernandez, G., Thornton, C., Stotland, A., Lui, D., Sin, J., Ramil, J., and Gottlieb, R. A. (2013). Novel tool for monitoring mitochondrial turnover MitoTimer. *Autophagy* **99**, 1852–1861.

Hoffmann, R. F., Zarrintan, S., Brandenburg, S. M., Kol, A., de Bruin, H. G., Jafari, S., and Heijink, I. H. (2013). Prolonged cigarette smoke exposure alters mitochondrial structure and function in airway epithelial cells. *Respir. Res*. **14**, 97.

Jia, L., Liu, Z., Sun, L., Miller, S. S., Ames, B. N., Cotman, C. W., and Liu, J. (2007). Acrolein, a toxicant in cigarette smoke, causes oxidative damage and mitochondrial dysfunction in RPE cells: Protection by (R)-alpha-lipoic acid. *Invest. Ophthalmol. Vis. Sci*. **48**, 339–348.

Joza, N., Susin, S. A., Daugas, E., Stanford, W. L., Cho, S. K., Li, C. Y. J., and Zu, J. C. (2001). Essential role of the mitochondrial apoptosis-inducing factor in programmed cell death. *Nature* **410**, 549–554.

Leboucher, G. P., Tsai, Y. C., Yang, M., Shaw, K. C., Zhou, M., Veenstra, T. D. and Weissman, A. M. (2012). Stress-induced phosphorylation and proteasomal degradation of mitofusin 2 facilitates mitochondrial fragmentation and apoptosis. *Mol. Cell* **47**, 547–557.

Lee, Y., Jeong, S. Y., Karbowski, M., Smith, C. L., and Youle, R. J. (2004). Roles of the mammalian mitochondrial fission and fusion mediators Fis1, Drp1, and Opa1 in apoptosis. *Mol. Biol. Cell* **15**, 5001–5011.

Li, H., Zhu, H., Xu, C. J., and Yuan, J. (1998). Cleavage of BID by caspase 8 mediates the mitochondrial damage in the Fas pathway of apoptosis. *Cell* **94**, 491–501.

Lin, Sabrina, and Talbot, P. (2011). Methods for Culturing Mouse and Human Embryonic Stem Cells. In: *Embryonic Stem Cell Therapy for Osteodegenerative Disease*, Humana Press, pp 31–56.

Martins-Green, M., Adhami, N., Frankos, M., Valdez, M., Goodwin, B., Lyubovitsky, J., and Curras-Collazo, M. (2014). Cigarette smoke toxins deposited on surfaces: Implications for human health. *PLoS One* **99**, e86391.

Matt, G. E., Quintana, P. J. E., Destaillats, H., Gundel, L. A., Sleiman, M., Singer, B. C., and Hovell, M. F. (2011). Thirdhand tobacco smoke: Emerging evidence and arguments for a multidisciplinary research agenda. *Environ. Health Perspect.* **119**, 1218–1226.

Mazzone, P., Tierney, W., Hossain, M., Puvenna, V., Janigro, D., and Cucullo, L. (2010). Pathophysiological impact of cigarette smoke exposure on the cerebrovascular system with a focus on the blood-brain barrier: Expanding the awareness of smoking toxicity in an underappreciated area. *Int. J. Environ. Res. Public Health* **77**, 4111–4126.

Meyer, J. N., Leung, M. C. K., Rooney, J. P., Sendoel, A., Hengartner, M. O., Kisby, G. E., and Bess, A. S. (2013). Mitochondria as a target of environmental toxicants. *Toxicol. Sci.* **134**, 1–17.

Newmeyer, D. D., and Ferguson-Miller, S. (2003). Mitochondria: Releasing power for life and unleashing the machineries of death. *Cell* **112**, 481–490.

Olichon, A., Guillou, E., Delettre, C., Landes, T., ArnaunÈ-Pelloquin, L., Emorine , L. J.,nd Belenguer, P. (2006). Mitochondrial dynamics and disease, OPA1. *Biochim. Biophys. Acta* **1763**, 500–509.

Otera, H., Ishihara, N., and Mihara, K. (2013). New insights into the function and regulation of mitochondrial fission. *Biochim. Biophys. Acta* **1833**, 1256–1268.

Rafalski, V. A., and Brunet, A. (2011). Energy metabolism in adult neural stem cell fate. *Prog. Neurobiol.* **93**, 182–203.

Rambold, A. S., Kostelecky, B., Elia, N., and Lippincott-Schwartz, J. (2011). Tubular network formation protects mitochondria from autophagosomal degradation during nutrient starvation. *Proc. Natl. Acad. Sci. U S A.* **108**, 10190–10195.

Ramsden, D. B., Ho, P. W. L., Ho, J. W. M., Liu, H. F., So, D. H. F., Tse, H. M., and Ho, S. L. (2012). Human neuronal uncoupling proteins 4 and 5 (UCP4 and UCP5): Structural properties, regulation, and physiological role in protection against oxidative stress and mitochondrial dysfunction. *Brain Behav.* **22**, 468–478.

Rehan, V. K., Sakurai, R., and Torday, J. S. (2011). Thirdhand smoke: A new dimension to the effects of cigarette smoke on the developing lung. *Am. J. Physiol. Lung Cell. Mol. Physiol.* **301**, L1–L8.

Rossignol, R., Gilkerson, R., Aggeler, R., Yamagata, K., Remington, S. J., and Capaldi, R. A. (2004). Energy substrate modulates mitochondrial structure and oxidative capacity in cancer cells. *Cancer Res.* **64**, 985–993.

Schick, S. F., Farraro, K. F., Perrino, C., Sleiman, M., van de Vossenberg, G., Trinh, M. P., and Balmes, J. (2014). Thirdhand cigarette smoke in an experimental chamber: Evidence of surface deposition of nicotine, nitrosamines and polycyclic aromatic hydrocarbons and de novo formation of NNK. *Tob. Control* **23**, 152–159.

Shen, Q., Yamano, K., Head, B. P., Kawajiri, S., Cheung, J. T. M., Wang, C., and van der Bliek, A. M. (2014). Mutations in Fis1 disrupt orderly disposal of defective mitochondria. *Mol. Biol. Cell* **25**, 145–159.

Shutt, T. E., and McBride, H. M. (2013). Staying cool in difficult times: Mitochondrial dynamics, quality control and the stress response. *Biochim. Biophys. Acta* **1833**, 417–424.

Squier, T. C. (2001). Oxidative stress and protein aggregation during biological aging. *Exp. Gerontol.* **36**, 1539–1550.

Stark, G. (2005). Functional consequences of oxidative membrane damage. *J. Membr. Biol.* **205**, 1–16.

Stridh, H., Orrenius, S., and Hampton, M. B. (1999). Caspase involvement in the induction of apoptosis by the environmental toxicants tributyltin and triphenyltin. *Toxicol. Appl. Pharmacol.* **156**, 141–146.

Sweeney, M. G., Bundey, S., Brockington, M., Poulton, K. R., Winer, J. B., and Harding, A. E. (1993). Mitochondrial myopathy associated with sudden death in young adults and a novel mutation in the mitochondrial DNA leucine transfer RNA(UUR) gene. *Q. J. Med.* **86**, 709–713.

Talbot, P., zur Nieden, N., Lin, S., Martinez, I., Guan, B., and Bhanu, B. (2014). Use of video bioinformatics tools in stem cell biology. In: *Handbook of Nanotoxicology, Nanomedicine and Stem Cell Use in Toxicology*, Eds: S. Sahu and D. Casciano, John Wiley, West Sussex, United Kingdom. Pp 379–402.

Tan, D., Goerlitz, D. S., Dumitrescu, R. G., Han, D., Seillier-Moiseiwitsch, F., Spernak, S. M., and Shields, P. G. (2008). Associations between cigarette smoking and mitochondrial DNA abnormalities in buccal cells. *Carcinogenesis* **29**, 1170–1177.

Tondera, D., Grandemange, S., Jourdain, A., Karbowski, M., Mattenberger, Y., Herzig, S., and Martinou, J. C. (2009). SLP-2 is required for stress-induced mitochondrial hyperfusion. *EMBO J.* **28**, 1589–1600.

Uttara, B., Singh, A. V., Zamboni, P., and Mahajan, R. T. (2009). Oxidative stress and neurodegenerative diseases: A review of upstream and downstream antioxidant therapeutic options. *Curr. Neuropharmacol.* **77**, 65–74.

van der Bliek, A. M. (2009). Fussy mitochondria fuse in response to stress. *EMBO J.* **28**, 1533–1534.

Wallace, K. B., and Starkov, A. A. (2000). Mitochondrial targets of drug toxicity. *Ann. Rev. Pharmacol. Toxicol.* **40**, 353–388.

Waris, G., and Ahsan, H. (2006). Reactive oxygen species: Role in the development of cancer and various chronic conditions. *J. Carcinog.* **55**, 14.

Yoon, Y., Galloway, C. A., Jhun, B. S., and Yu, T. (2011). Mitochondrial dynamics in diabetes. *Antioxid. Redox Sign.* **14**, 439–457.

Zahedi, A., Phandthong, R., On, V., and Talbot, P. (2015). A novel video bioinformatics toolbox to study mitochondrial morphology, dynamics, and mitophagy in stressed stem cells. In *Proceedings of Annual American Society of Cell Biology, San Diego, California, December 2015*. San Diego, *Am. Soc. Cell Bio.* E37.

Zanna, C., Ghelli, A., Porcelli, A. M., Karbowski, M., Youle, R. J., Schimpf, S., and Carelli, V. (2008). OPA1 mutations associated with dominant optic atrophy impair oxidative phosphorylation and mitochondrial fusion. *Brain* **131**, 352–367.

Zhang, J., Khvorostov, I., Hong, J. S., Oktay, Y., Vergnes, L., Nuebel, E., and Teitell, M. A. (2011). UCP2 regulates energy metabolism and differentiation potential of human pluripotent stem cells. *EMBO J.* **30**, 4860–4873.

Ziech, D., Franco, R., Pappa, A., and Panayiotidis, M. I. (2011). Reactive oxygen species (ROS)–induced genetic and epigenetic alterations in human carcinogenesis. *Mutat. Res.* **711**, 167–173.